

Development of Requirements for Resistance Spot Welding Dual-Phase (DP600) Steels Part 2: Statistical Analyses and Process Maps

Weld diameter proved to be the primary factor influencing type of weld fracture

BY M. MARYA AND X. Q. GAYDEN

ABSTRACT. The DP600 steels have presented new challenges to the conventional practice of resistance spot welding. In developing process requirements to spot weld stacks of two identical DP600 steel sheets, a statistical method was applied in order to establish empirical relationships between the type of weld fracture during quality control (i.e., interfacial vs. button pullout), the weld current, the weld time, and the sheet thickness independent of chemical composition and galvanized coating. The selected methodology was so successful that maps to select process parameters were developed for spot welding 0.9- to 2.2-mm-thick DP600 steels. This study also confirmed that weld diameter was a primary factor influencing type of weld fracture. A new relationship between minimum weld diameter to prevent interfacial fracture during quality control and sheet thickness was also determined, and compared with several resistance spot weld standards.

Introduction

In the automotive world, increasing demands regarding weight, safety, and cost have led to the introduction of the so-called advanced high-strength steels (AHSS) (Refs. 1, 2). These relatively new steels rival the light metals and the composites due to cost advantages and the fact that the vehicle manufacturing infrastructures for steels may still be utilized. Ranked in order of increasing strength, the most common advanced high-strength steels include dual-phase (DP) steels, complex-phase (CP) steels, transformation-induced plasticity (TRIP) steels, and martensitic (MART) steels (Ref. 1). The mechanical properties of DP steels are achieved using well-defined cooling

schedules from the austenite or the ferrite+austenite region; i.e., schedules in which austenite is first transformed to ferrite, before a rapid cooling that transforms the remaining austenite to martensite.

Resistance spot welding of DP600 steels (i.e., dual-phase steels with 600-MPa ultimate tensile strength) (Refs. 1, 2) has been challenging because of the frequent occurrence of weld interfacial fractures during quality control by the chisel test (Ref. 3). The type of weld fracture (i.e., interfacial vs. button pullout) that develops during testing depends upon several major factors. In Part 1 of this study with two DP600 steels (Ref. 3), sheet thickness (gauge) and weld diameter were identified as two primary factors influencing weld fracture, while the steel chemical compositions were of no measurable effect. Although the role of chemical composition was not yet entirely clarified with DP600 steels, the mechanical properties of the as-received steels include factors that influence weld fracture with various steel grades (Ref. 4), and that is simply due to the fact that various microstructures and sets of properties can be generated from a single composition. In addition to these factors, all related to the materials, spot weld fracture is also affected by the test loading conditions (Refs. 4, 5). As an example, in the first part of this study, many spot welds that did produce the so-called "weld buttons" during the chisel test were seen to fracture interfacially during the quasistatic tensile-shear test (Ref. 3). Test sample geometry and dimensions, as well as rate of loading, are other factors that can greatly influence weld fracture (Refs. 4, 5).

As illustrated in Fig. 1, the chisel test has similarities with the mode-I fracture toughness test where the unbound interface around the weld fusion zone acts as a circumferential notch. However, unlike the fracture toughness test, where a triaxial stress state is guaranteed by the sample geometry to cause a planar fracture, the chisel test allows cracking from the fusion zone periphery to grow inward, and induce an interfacial fracture, or to deflect and create a weld button — Fig. 1. In this second paper, the focus is placed on the process conditions that eliminate weld interfacial fracture during the chisel test. In contrast with Part I of this study, which was restricted to only two steels (Ref. 3), a number of commercial DP600 steels in a wide range of gauges were included. In order to process the increasing amount of experimental data, a robust statistical methodology was applied so that predictive equations and process maps (to select process parameters) could be developed for all DP600 steels (regardless of their supply origins). Having the repeatability of the chisel test established (Ref. 3), this methodology based on statistical analyses of chisel test results was justified, and could therefore be applied to generate guidelines for the spot welding of DP600 steel sheets.

Searching for Fit Functions

To facilitate the analyses of the weld data, mathematical relationships between process parameters (i.e., weld current and weld time) and sheet thickness (gauge) were searched, assuming that other factors, such as chemical composition and coating conditions were secondary (Ref. 3). To determine relationships between process variables, the two limiting events for spot welding galvanized steels (i.e., the onset of melting for the steel and the onset of expulsion for the zinc, which precedes that of the steel) were used in conjunction with heat conduction models for instantaneous heat sources (Refs. 6, 7). According to the well-known Rosenthal models, the

M. MARYA, formerly with the G. S. Ansell Department of Metallurgical and Materials Engineering, Colorado School of Mines, Golden, Colo., is now with Schlumberger Reservoir Completions, Rossharon, Tex. X. Q. GAYDEN is with Materials and Process Laboratory, General Motors Research and Development, Warren, Mich.

KEYWORDS

Dual-Phase 600 Steels (DP600)
Resistance Spot Welding
Process Maps
Minimum Weld Diameter
Interfacial Fracture

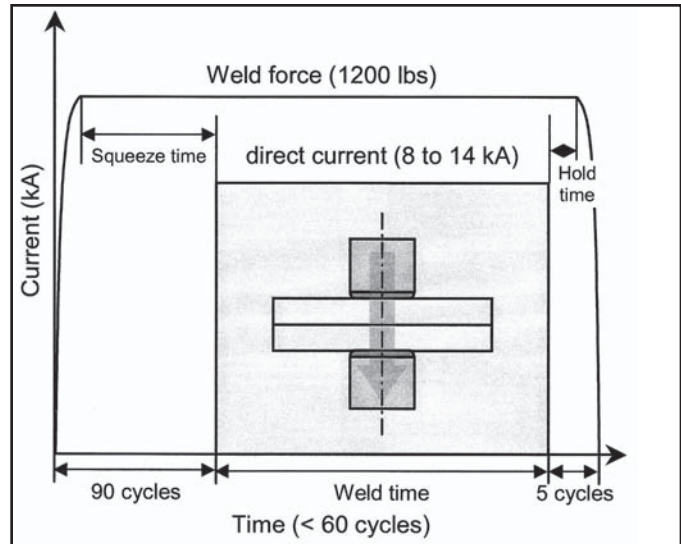
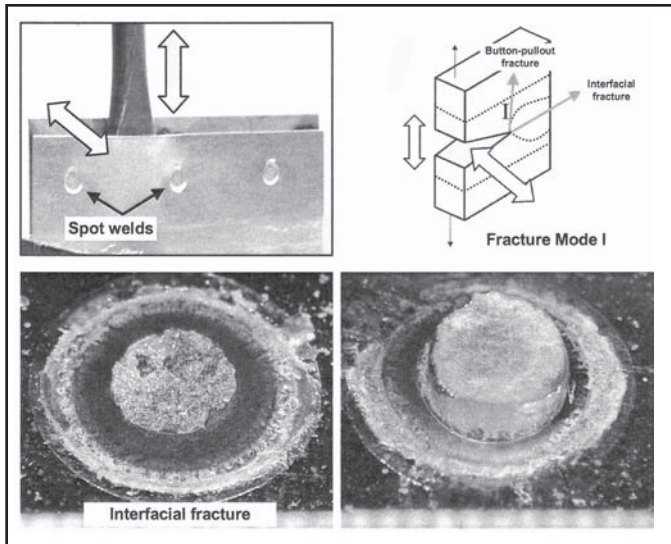


Fig. 1 — Description of the chisel test, analogy with a fracture mode-I test, and the two major types of weld fracture seen during the test.

Fig. 2 — Schematic representation of the weld schedules selected for this investigation.

field of temperatures caused by an instantaneous moving heat source, either represented by a point at the surface to be melted (3-D heat conduction), a line (2-D heat conduction), or a plane (1-D heat conduction) passing through the entire thickness can be described as follows:

$$T = T_0 + \frac{\left(\frac{Q}{d^{\text{dim}}}\right)}{\rho \cdot C \cdot (4\pi \cdot a \cdot t)^{\text{dim}/2}} \exp\left[-\left(\frac{r}{2 \cdot a^{1/2} \cdot t^{1/2}}\right)^2\right] \quad (1)$$

where Q is the power of the heat source (directly related to weld current, I), d is the material thickness, ρC is its volumetric specific heat, r is the distance from the heat source where the temperature, T , is estimated by incrementing the initial temperature, T_0 , and “dim” designates the number of dimensions (1 to 3) associated with the selected heat source. Depending upon process parameters and sheet thickness, both two- and three-dimensional models can approximate thermal cycles experienced by resistance spot welds. Thermal cycles corresponding to shallow welds fit the three-dimensional solution better (dim = 3), while the two-dimensional solution (dim = 2) is more appropriate for melt-through welds.

When temperature, T , and position, r , are fixed, note that Equation 1 is reduced from three independent variables, t , d , and Q , to two, which means that a mathematical relationship between weld time, t ,

sheet thickness, d , and heat source power, Q , can be determined. From Equation 1, t , d , and Q can be compared with a common quantity such as the distance, r . If distance is fixed to a constant value, it becomes apparent that t , d , and Q are related to each other by nonlinear relationships. The time, t , associated with temperatures of incipient melting or beginning of expulsion is thus likely described by the other parameters as follows:

$$t = a \cdot d^b \cdot I^c \quad (2)$$

where a , b , and c are to be estimated through statistical analyses, particularly a least-square root regression. In Equation 2, b has a positive value (i.e., the greater the thickness d , the longer the time t), whereas c is negative (i.e., the higher the current, the smaller the time to produce either incipient melting or expulsion), and its absolute value is expected to approach 2, a value normally associated with the Joule heating of a resistor.

It is clear that countless analytical relationships between the process parameters can describe well incipient melting, beginning of expulsion, or any other physical phenomena during spot welding. Recall that in Equation 1, the distance, r , is coupled with an exponential term. By analogy, thickness, d , can be attached to an exponential function, as given by Equation 3. This change over Equation 2 increases the role of thickness relative to that of the other variables, which is a possibility that had to be considered in view of past experimental observations that sheet thickness was a primary factor in influencing weld fracture (Ref. 3).

$$t = a \cdot \exp(b \cdot d) \cdot I^c \quad (3)$$

A least-square root minimization of the deviation between experimental data and fit function data was therefore needed to determine which of Equations 2 and 3 fit the experimental data better, or if new and more complex mathematical representations were needed. With both Equations 2 and 3, the evaluation of least-square root constants, a , b , and c , was facilitated by introducing a logarithmic transformation so that the new transformed equation becomes a linear function of known quantities, here d and $\ln(I)$.

$$\ln(t) = \ln(a) + b \cdot d + c \cdot \ln(I) \quad (4)$$

where $\ln(a)$, b , and c are the three new constants to be evaluated using three independent but linear equations. Assuming that the total number of experimental data points is “ n ” and “ i ” is an integer between 1 and “ n ,” the difference between the predicted value of time corresponding to the i^{th} data point (Equation 3) and its measured value, t_i , had to be minimized for all the data points. The α function, presented as Equation 5, is the sum of the differences squared between the measured time, t_i , and the calculated time, t .

$$\alpha = \sum_{i=1}^n \left[\ln(a) + b \cdot d_i + c \cdot \ln(I_i) - \ln(t_i) \right]^2 \quad (5)$$

To determine the three unknown regression constants, the α function was minimized; i.e., all its first partial derivatives were zeroed, exactly as follows:

$$\frac{\partial \alpha}{\partial \ln(a)} = 0 \quad (6)$$

$$\frac{\partial \alpha}{\partial b} = 0 \quad (7)$$

$$\frac{\partial \alpha}{\partial c} = 0 \quad (8)$$

By developing Equations 6–8 and using a matrix notation, the three unknowns, $\ln(a)$, b , and c were evaluated after multiplying the left term of the following equation by the 3×3 reciprocal matrix.

$$\begin{bmatrix} \sum_{i=0}^{n \text{ data points}} d_i^2 & \sum_{i=0}^{n \text{ data points}} d_i \ln(I_i) & \sum_{i=0}^{n \text{ data points}} d_i \\ \sum_{i=0}^{n \text{ data points}} d_i \ln(I_i) & \sum_{i=0}^{n \text{ data points}} [\ln(I_i)]^2 & \sum_{i=0}^{n \text{ data points}} \ln(I_i) \\ \sum_{i=0}^{n \text{ data points}} d_i & \sum_{i=0}^{n \text{ data points}} \ln(I_i) & n \end{bmatrix} \begin{bmatrix} b \\ c \\ \ln(a) \end{bmatrix} = \begin{bmatrix} \sum_{i=0}^{n \text{ data points}} d_i \ln(t_i) \\ \sum_{i=0}^{n \text{ data points}} \ln(I_i) t_i \\ \sum_{i=0}^{n \text{ data points}} t_i \end{bmatrix} \quad (9)$$

In developing empirical equations, high correlation coefficients and small residual values were primary to decide whether a particular equation (here selected to be Equation 3) could be applied or not. The correlation coefficient, r_c , and the coefficient of determination, r_c^2 , which both measure the deviation between the actual and the calculated values, were computed using Pearson's formula (Ref. 8). Successful fit functions were those that provide coefficients as close to one as possible. A value of 0.9 for r_c^2 (for instance) meant that the variance was at 90% explained by the fit function, while the remainder was attributed to the inadequacy of fit function and measurement scatter. The correlation coefficient between measured, t_i , and calculated time with any of the selected fit equation, t_{cal} , was calculated as follows:

$$r_c = \frac{\sum_{i=0}^n t_i t_{cal} - \frac{\sum_{i=0}^n t_i \sum_{i=0}^n t_{cal}}{n}}{\left(\left[\sum_{i=0}^n t_i^2 - \frac{\left(\sum_{i=0}^n t_i \right)^2}{n} \right] \left[\sum_{i=0}^n t_{cal}^2 - \frac{\left(\sum_{i=0}^n t_{cal} \right)^2}{n} \right] \right)^{-1/2}} \quad (10)$$

Empirical relationships to predict weld button diameter as a function of weld current, weld time, and sheet thickness were developed using a similar methodology, in which well-established heat-flow models dictated the shape of the fit function (Refs. 6, 7). Of the three heat transfer mechanisms during resistance spot welding (conduction, convection, and radiation), heat extraction away from the weld pool by conduction through the sheet is the dominant mechanism (Ref. 7). Similar to mass diffusion problems (Ref. 7), assuming that thermal conduction controls the dimensions of the weld pool, weld growth may be modeled directly by Equation 11, and if not, surely by a highly similar equation. The selection of Equation 11, or closely similar equations, was in line with results from the first study, and other studies where weld diameter was seen to increase with time and current at rates that decreased with weld diameter (Refs. 3, 9). Since weld pool diameters and weld button diameters are closely related, Equation 11 was extended to describe the evolution of the weld button with the process variables, I and t , and the sheet thickness, d .

$$\phi = F(d, I) \cdot t^n \quad (11)$$

In Equation 11, ϕ was thus defined as the button diameter, F was an unknown func-

tion of both the sheet thickness and the weld current, and n was a growth constant. In reference to mass diffusion problems, where the driving force (then the gradient in chemical potentials) decreases linearly with time due to thickening, the expected value for n was $\frac{1}{2}$ (Ref. 7). If Equation 3 is proven to be a good fit for the measured values of weld time, then similarities between the function F in Equation 11 and Equations 2 and 3 may be anticipated, and a fairly complete description of ϕ may be found by expanding Equation 11 as follows:

$$\phi = \sum_i a_i \cdot \exp(b_i) I^{c_i} \cdot t^{n_i} \quad (12)$$

where i is an integer to be determined. For practical purposes, the number of added terms in Equation 12 (given by i) was held as small as necessary.

Experimental Procedure

Table 1 lists all seven commercial DP600 steels that were selected for this study. Note that all DP600 steels were hot-dipped galvanized, and that no steel was identical to another as both chemical compositions and gauges varied noticeably. In Table 1, and in the remainder of this paper, note that the steels were designated using the values of their gauges and not their trade names, which have been kept confidential.

For this study, the welding parameters were as described in Fig. 2, and thus similar to those selected in the first part of this study (Ref. 3). The sheets were also sheared into 38-mm-wide and 127-mm-long coupons and welded in stacks of two identical coupons using a mid-frequency DC welding machine. On each stack, three equally spaced welds were produced from the coupon center, as shown in the upper-left image of Fig. 1. To create a diversity of weld dimensions (especially diameters), weld current and weld time were, respectively, varied from 8 to 12 kA and 2 to 40 cycles. Unlike weld current and weld time, the weld force, squeeze time, and hold time were respectively kept constant at

Table 1 — List and Chemical Compositions (in wt-%) of the DP600 Steels Used in This Investigation

Material	Gauge	C	Mn	Si	Mo	Cr	Ni	Ti	V	Al	Sn	P	S
DP09	0.95 mm	0.096	1.500	0.100	0.260	0.020	0.010	0.010	—	0.030	—	0.020	0.010
DP10	1.00 mm	—	—	—	—	—	—	—	—	—	—	—	—
DP14	1.42 mm	0.080	1.800	0.010	0.159	0.220	0.010	0.001	0.001	0.032	0.002	0.017	0.007
DP16	1.67 mm	0.093	1.560	0.160	0.140	0.032	0.003	0.005	0.003	0.040	0.004	0.033	0.004
DP18	1.80 mm	0.120	1.450	0.400	0.060	0.210	0.010	0.000	—	0.020	0.010	0.010	0.010
DP20	2.00 mm	0.098	1.580	0.198	0.005	0.281	0.022	0.003	0.060	0.057	0.008	0.015	0.003
DP22	2.22 mm	0.070	1.830	0.015	0.187	0.190	0.010	0.001	0.001	0.042	0.004	0.014	0.007

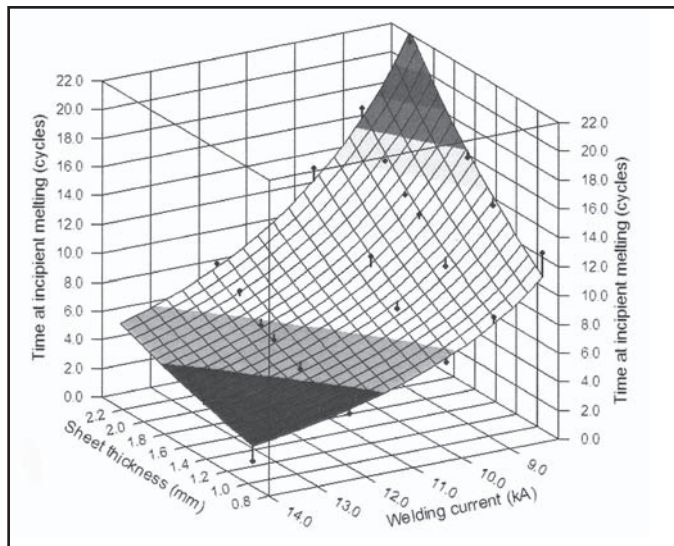


Fig. 3 — Three-dimensional representation suggesting a relationship between current, weld time, and sheet thickness at incipient melting.

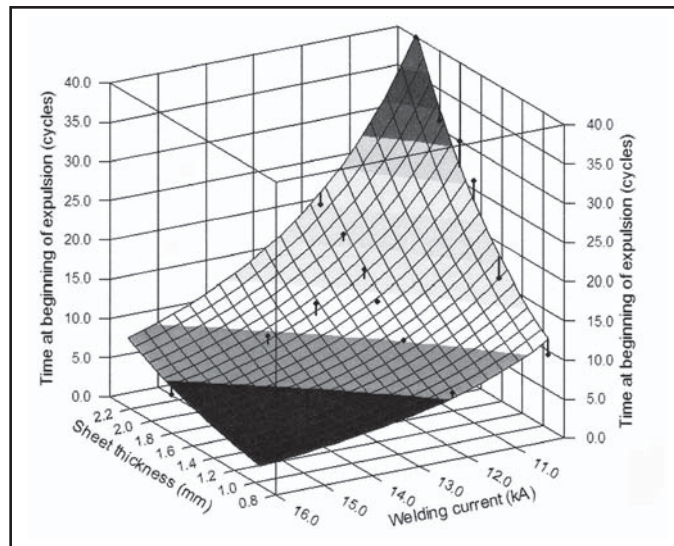


Fig. 4 — Three-dimensional representation suggesting a relationship between current, weld time, and sheet thickness at the beginning of zinc expulsion.

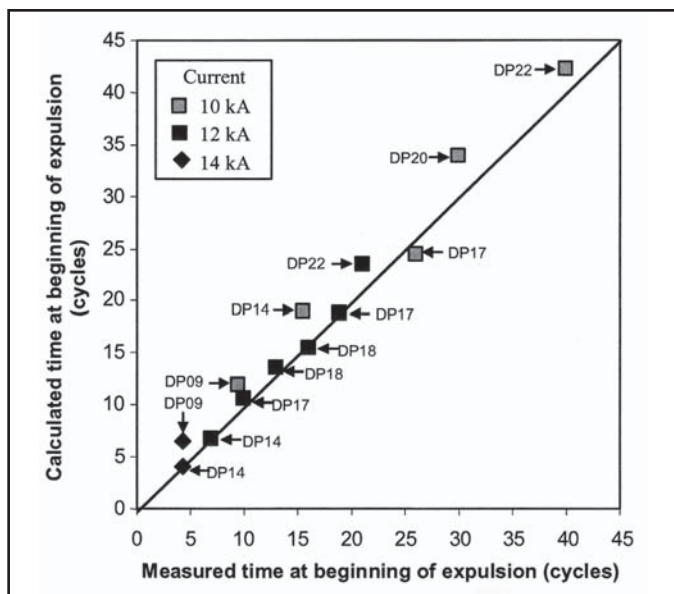


Fig. 5 — Graphical representation showing an excellent correlation between measured time and calculated time (Equation 13) at the beginning of expulsion for various currents and steels.

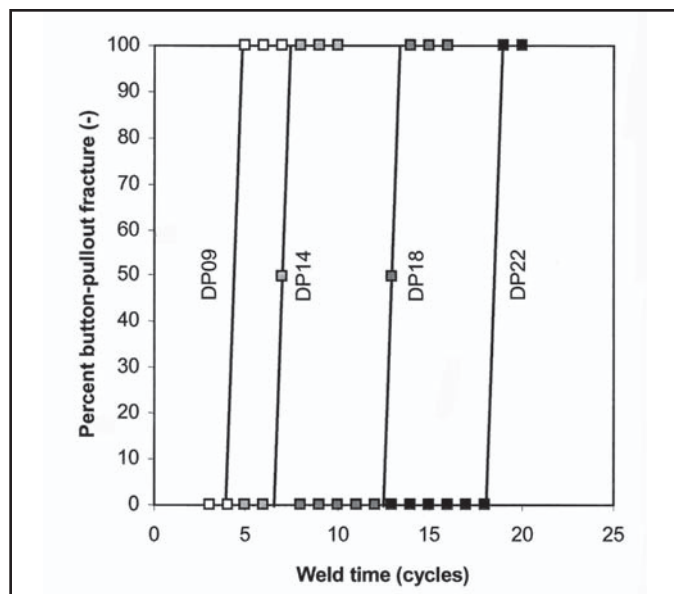


Fig. 6 — Percent button-pullout fracture vs. weld time for various steels (12-kA current).

1200 lb (5.3 kN), 90 cycles, and 15 cycles. The caps (5.0-mm face diameter) that were placed at the end of each water-cooled electrode were regularly replaced to prevent cap wear from altering weld characteristics, in particular, dimensions. On average, the caps were replaced after 60 to 80 welds depending upon the process parameters — a replacement that was certainly far more frequent than in a production environment.

All resistance spot welds were fractured using a hand-held pneumatic chisel (Ref. 10). All weld button diameters were measured several times before being averaged and incorporated in any data analyses. Each stack of two coupons provided

two identical spot welds, in addition to the central shunt weld. This shunt weld was not considered unless discrepancies between the other two welds were encountered. Finally, since all welds were produced using a single pulse of current (its duration being the weld time), the effects of preheating and tempering pulses were not addressed in this study (Ref. 11).

Results and Discussion

Relationships between Process Parameters

The contributions of process variables such as current and time (in cycles) were

simultaneously investigated to identify relationships involving both variables with sheet thickness. To this purpose, time to reach incipient melting and time to reach zinc expulsion were measured using the various DP600 steels of Table 1. Time for incipient melting was determined by gradual increments of 1 or 2 cycles (depending upon current) until some fusion underneath the zinc coating could be observed. As demonstrated in the forthcoming figures, this methodology provided consistent results with negligible and inconsequential measurement errors.

In Fig. 3, measured time to reach incipient melting is depicted as a function of sheet thickness and weld current. In addi-

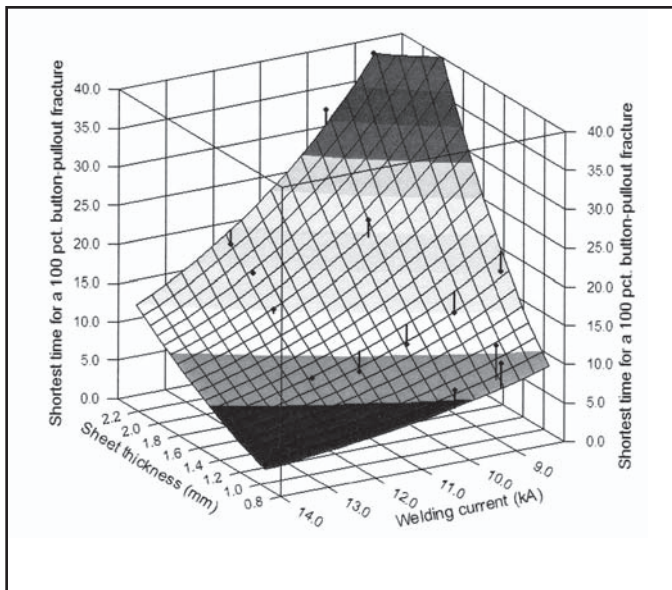


Fig. 7 — Three-dimensional representation showing the minimum weld time required for consistent button-pullout fracture using different currents and sheet thicknesses.

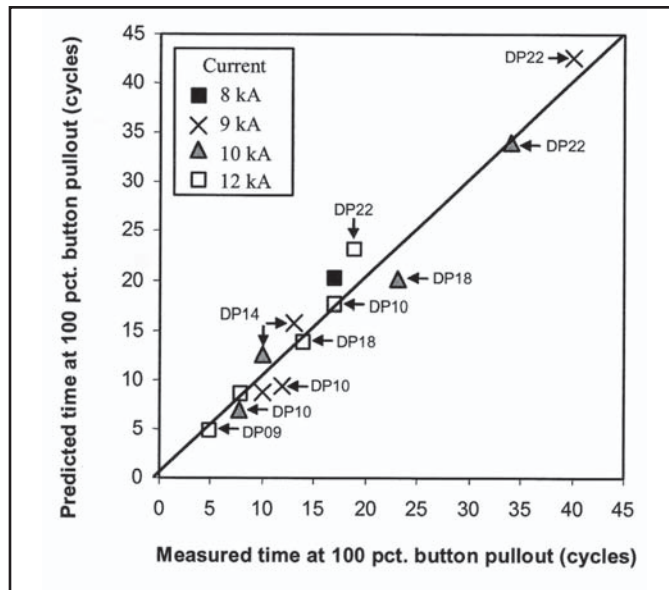


Fig. 8 — Graphical representation showing another excellent correlation between calculated for consistent button-pullout fracture time (Equation 14) and measured time.

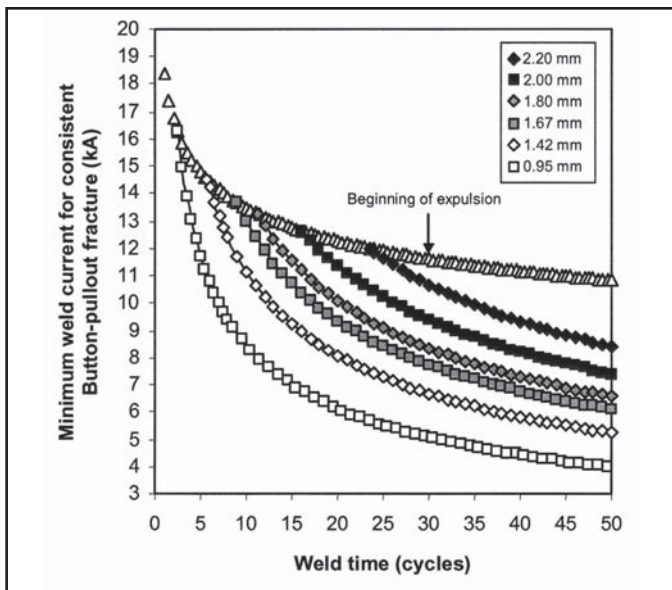


Fig. 9 — Process map showing current and weld time requirements for producing consistent button-pullout fractures during chisel testing. Process parameters must be selected such that they are above the lower line for a given gauge, but lower than the expulsion line.

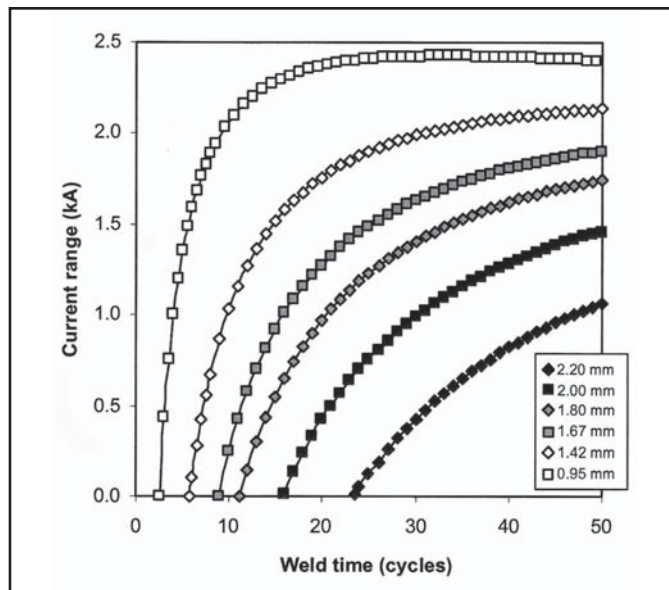


Fig. 10 — Process map showing the current range to produce consistent button-pullout fracture without causing expulsion.

tion to an evident functionality between time to melting and both sheet thickness and weld current, the fit surface (a representation of Equation 3) is seen to pass through the experimental data points with negligible deviation. This infers that an excellent correlation exists between the selected variables and the measured values of the time at incipient melting, and that none of the unaccounted parameters have an effect, at least on the heat transfer preceding melting. The excellent results of Fig. 3 also validate that neither variations in electrical resistance from chemical

composition or zinc coatings, nor changes in contact resistance between surfaces were of influence. If any of these parameters influenced heat transfer, their roles were clearly concealed within the measurement scatter, and thus negligible. Sheet thickness was the only parameter that could substantiate the differences seen between the different DP600 steels.

In Fig. 4, the time to reach expulsion is used as substitute to the time at incipient melting found in Fig. 3. Due to the resemblance between Figs. 3 and 4, similar relationships between the variables shown on

both figures were expected, and consequently the use of Equation 3 was logically extended to calculate time to expulsion. Because expulsion is an important event that restricts process parameter selection, the least-square root fit represented by the surface of Fig. 4 needed to be quantified. By repeating the process described in Section 2, Equation 13 was obtained with a coefficient of correlation of 0.97. Also, judging from the limited deviation between the fit surface and the measured data points, Equation 13 was considered to be nearly perfect to calculate the minimum weld

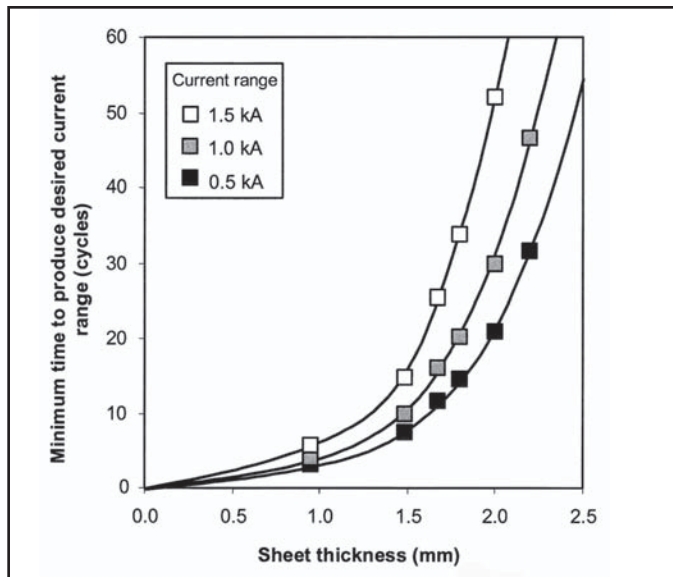


Fig. 11 — Minimum weld time to obtain a desired current range for producing weld buttons without zinc expulsion vs. sheet thickness.

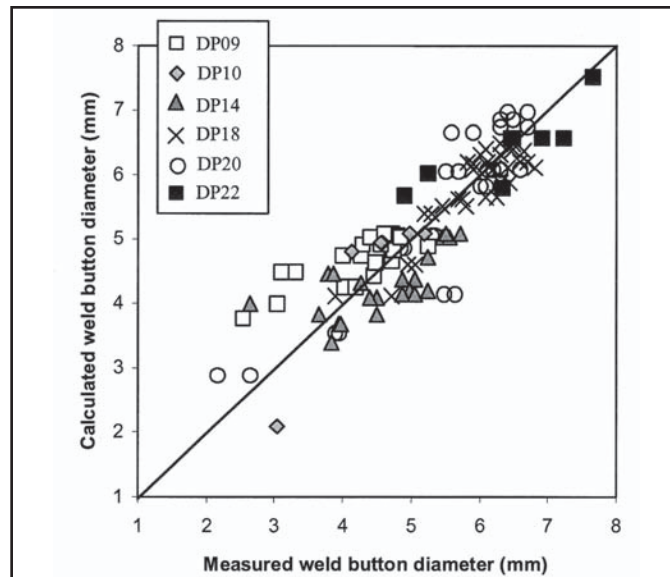


Fig. 12 — Comparison between measured and calculated weld button diameters (Equation 15).

time at beginning of zinc expulsion.

$$t_{\text{Expulsion}} = 7252 \cdot \exp(d) \cdot I^{-3.2} \quad (13)$$

In Equation 13, as in the upcoming equations, t designates the time, d is the sheet thickness, and I is the current. Figure 5, which compares measured time and time calculated with Equation 13, reveals that the data are in excellent agreement. Equation 13 also demonstrates that melting did not require a more complex mathematical description, a possible confirmation that the convection within the weld pool might not play any major role in the overall heat transfer. As for the onset of melting, any possible contributions from the chemical composition were hidden within the scatter of the experimental measurements. Finally, note that the exponent for the current was 1.6 times greater than the expected value of -2 .

With the interactions between the process parameters and the sheet thickness clarified, the problem of weld interfacial fracture was revisited. Figure 6 confirms that increasing the weld time rapidly changes the type of weld fracture from interfacial to button pullout, as already established in the first study (Ref. 3), and explained by weld diameter (Refs. 3–5). Figure 6 also demonstrates that all DP600 steels can pass the chisel test given sufficient weld time. Figure 7 shows the minimum weld time to consistently produce button-pullout fractures for various currents and gauges. With Equation 3 to mathematically represent the surface of Fig. 7, the following equation was also obtained with a coefficient of correlation of 0.97:

$$t_{100\% \text{ but.}} = 280 \cdot \exp(1.25 \cdot d) \cdot I^{-2.12} \quad (14)$$

Unlike Equation 13, note that the exponent associated with the current in Equation 14 is much closer to the absolute theoretical value of 2. The dependence on the thickness is also greater in Equation 14, as indicated by the coefficient of 1.25 in the exponential term. The two empirical equations, therefore, strongly suggest that expulsion is less controlled by the thickness and more by the current than incipient melting. This result is not totally counterintuitive because expulsion is an interfacial phenomenon, thus primarily related to the contact properties (thus resistance and Joule heating) and less by the thickness, while the time to create welds that consistently make buttons during testing relates to the weld diameter, which is more affected by the bulk of the material, thus the sheet thickness, and less by the Joule heating from the contacting sheet surfaces (Refs. 12, 13).

Figure 8 compares calculated and measured values of minimum weld time to fully eliminate interfacial fracture. As for Equation 13, the correlation obtained between Equation 14 and the experimental measurements was excellent. Having both Equations 13 and 14 validated, process maps such as those of Figs. 9 and 10 were generated for weld schedules like in Fig. 2. For combinations of weld time and sheet thickness, the minimum weld currents to eliminate interfacial fracture were calculated to generate a set of constant-thickness lines. By equating the variable for the time in Equations 13 and 14, the expulsion currents were also determined for specific values of sheet thickness. The result of a series of such calculations is the upper line in Fig. 9, a line that depicts the expulsion current — sheet thickness relationship

and transposed it on a weld time — weld current representation.

The maps of Figs. 9 and 10 show the process parameters to produce spot welds in DP600 that are guaranteed to resist interfacial fracture in the chisel test. Although developed for single-pulse DC schedules, these maps can be generalized and extended to other weld schedules as the relationship between sheet thickness and process parameters is unlikely to vary to great extents. Figures 9 and 10 clearly demonstrate how the sheet thickness severely restricts the selection of the process parameters. For the welds of this study, Fig. 9 shows that the 0.95-mm-thick steel will produce buttons even with a 5-cycle weld time providing that current is 12 kA at the very minimum. In contrast, the 2.20-mm-thick steel will necessitate weld times of at least 30 cycles to ensure the formation of a button, and the corresponding currents will have to exceed 9 kA.

The range of available currents to produce weld buttons without expulsion is an indication of the process robustness. This range is simply defined by the difference between the minimum current to produce a weld button and the expulsion current. Large current ranges are necessary because they raise the chances of process parameter overlaps between different materials, they reduce the need for altering welding procedures for new materials, and they make the welding process robust, i.e., insensitive to materials variations. Due to its practical significance, both Figs. 10 and 11 describe the current range, as calculated by combining Equations 13 and 14.

Figure 10 first indicates that current range decreases rapidly with the sheet thickness, and gradually levels off as the

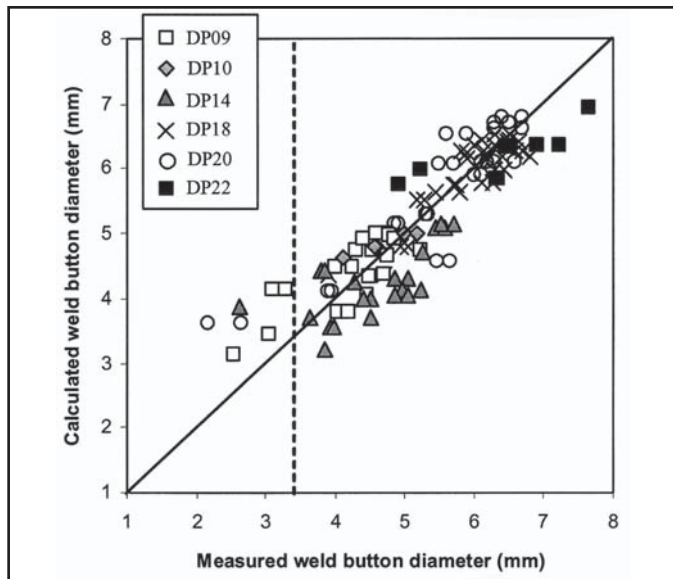


Fig. 13 — Comparison between predicted weld button diameters vs. measured weld button diameters (Equation 16).

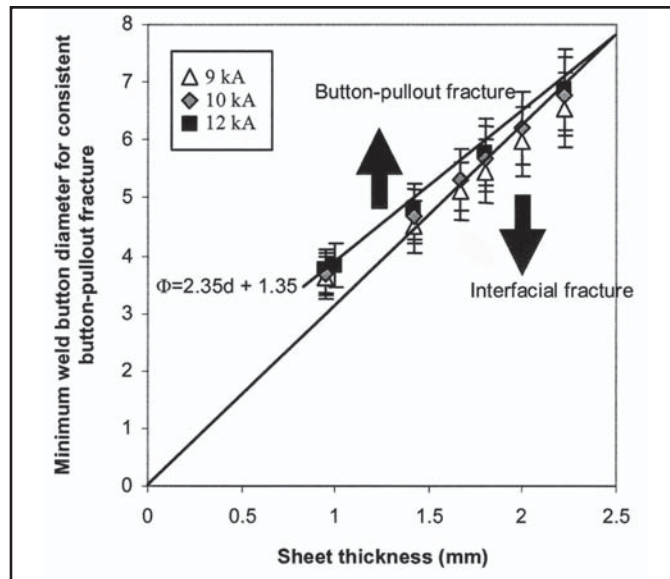


Fig. 14 — Minimum weld button diameter for consistent button-pullout fracture vs. sheet thickness with 9-, 10-, and 12-kA currents. While contribution of current is secondary, weld button diameter mainly controls the type of fracture during chisel testing.

weld time increases. According to Fig. 10, a current range of 1.8 kA (a value sometimes considered minimum to ensure a good process robustness (Ref. 9)) will unlikely be found for sheets that are 1.6 mm and thicker. Figure 11, which plots horizontal sections of Fig. 10 at current ranges of 0.5, 1.0, and 1.5 kA, shows for several gauges the minimum weld time to produce a desired current range (for the corresponding currents, see Fig. 9). This figure also illustrates that the contribution of the sheet thickness is exponential, as indicated by Equations 13 and 14. For spot welding, this means that welding will become increasingly sensitive to variations in sheet thickness as the sheets thicken. Since thickness considerably affects heat conduction (e.g., 2-D vs. 3-D heat flow (Ref. 7)), any factor that would affect heat conduction even slightly (e.g., coating thickness, coating composition, and steel chemical composition) is also likely to affect weld fracture. Therefore, with heavy gauges, variations in steel composition between different DP600 steels are predicted to become important factors to take into account when developing guidelines to spot weld DP600 steels.

Weld Button Diameters

More than 300 weld button diameters were measured for the least-square root analyses. Despite occasional major variations between welds produced with identical process parameters, empirical correlations were still successfully established. Equation 15 provides an acceptable description of the weld button diameter, Φ , as a function of weld current, I , and sheet

thickness, d . Using the approach described previously, Equation 15 was obtained with a correlation coefficient of 0.86.

$$\phi_1 = 4.96 - 15.83 \cdot \exp(0.872 \cdot d) \cdot I^{-0.62} + 0.967 \cdot \exp(0.216 \cdot d) \cdot I^{-0.642} t^{0.769} - 0.22 \cdot I \cdot t \quad (15)$$

Based upon series of calculations, it was determined that the summation of three short functions was minimal to reach a satisfactory correlation with the measured weld button diameters. Figure 12 compares measured and calculated weld button diameters using Equation 15. Although the trend in Fig. 12 is accurate, the data are substantially dispersed, particularly when weld button diameter is less than 3.5 mm. In order to avoid underestimating weld button diameters with small welds, another empirical model was developed by correcting Equation 15 for the large scatter seen with small welds. To reduce scatter, a linear correction was superimposed, i.e., the diameter in Equation 15 became the input parameter in Equation 16.

$$\phi_2 = (2.04 - 0.63 \cdot d) \phi_1 + (3.5d - 5.65) \quad (16)$$

As illustrated in Fig. 13, Equation 16 did not improve the correlation. The scatter remained as large as 20%, particularly when weld button diameter was greater than 3.5 mm (i.e., for those welds that are on the right of the dash line of Fig. 13). Improving the predictability of the selected fit function was considered unfeasible and mainly limited by the accuracy of the measurements.

Of practical significance, both Equations 15 and 16 were used conjointly with Equation 14 to determine minimum weld button diameters to fully eliminate weld interfacial fracture. By inserting into either Equation 15 or 16 the value of minimum weld time, given by Equation 14 for zero interfacial fracture, a minimum weld button diameter could be determined for each combination of process parameters. Figure 14 presents the results of this calculation and stresses two important points. First, the current has a negligible effect on the minimum weld button diameter against interfacial fracture. Second, this minimum weld button diameter increases linearly with the sheet thickness. Because current has no real effect on minimum weld button diameters, past correlations between minimum weld button diameter and sheet thickness became entirely substantiated (Refs. 14, 15). To prevent weld interfacial fractures during chisel testing and to assist the selection of the process parameters, the following relationship, which fits the majority of the data points of Fig. 14, was also developed:

$$\phi_{100\% \text{ button}} = 2.35d + 1.35 \quad (17)$$

Due to the scatter encountered in Fig. 13, well represented by Fig. 15, a more conservative equation, where values from previous equations have been increased by about 15%, is also proposed:

$$\phi_{100\% \text{ button}} = 2.7d + 1.6 \quad (18)$$

With the proposed oversizing, only a few welds among the 300 tested welds were found to produce interfacial fractures.

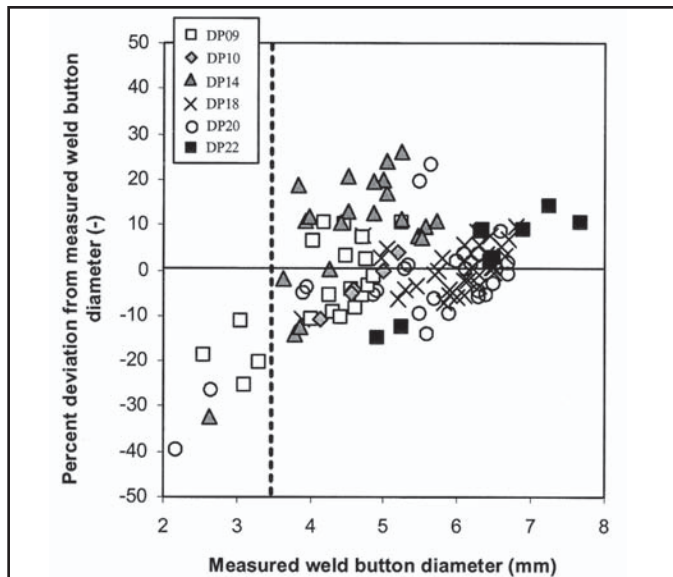


Fig. 15 — Graphical representation showing the scatter seen in Fig. 13. Predicted weld button diameters are within 20% of the measured values.

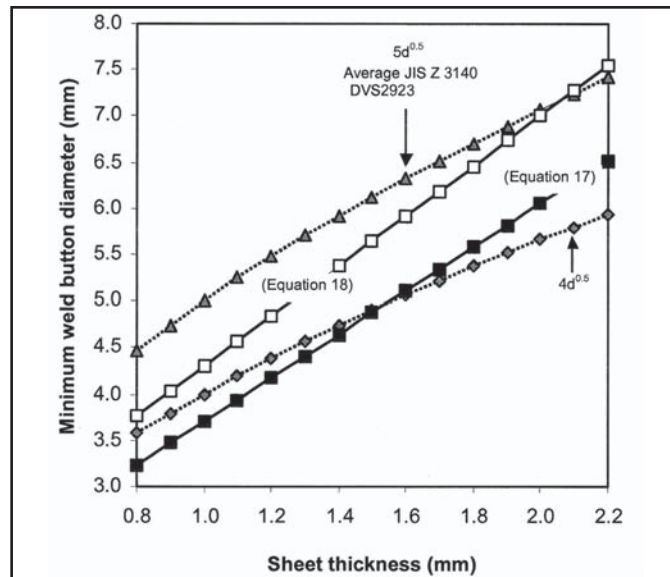


Fig. 16 — Comparison of minimum weld button diameters, as given by specifications (Refs. 14, 15) and as recommended by this study.

With rare exceptions, all resistance spot welds satisfying Equation 18 produced weld buttons during the chisel test. Equation 18 can therefore be considered as a reliable replacement to Equation 17.

For practical purposes, the minimum weld button diameters given by Equation 17 were compared to those recommended by existing standards, specifically the Japanese JIS Z3140 and the German DVS2923 standards (Refs. 14, 15). Figure 16 indicates that the well-known $4 \cdot d^{0.5}$ rule of thumb applies quite well to DP600 resistance spot welds as long as sheet thickness is less than 1.5 mm. Beyond 1.5 mm, this rule becomes less applicable. In Fig. 16, the values from Equation 17 closely approximate the values from the $5 \cdot d^{0.5}$ rule, recommended by the Japanese and German standards (Refs. 14, 15). Equation 17 and the $5 \cdot d^{0.5}$ rule are most appropriate when the DP600 steel thickness exceeds 1.5 mm. When comparing this result with the minimum weld diameters in traditional steel spot welding, the study shows that DP600 steels required larger welds, in particular for the heavier gauges. As investigated in a more recent paper (Ref. 4), a more complete and refined description of weld fracture needs to take into account additional factors, especially the mechanical properties associated with the initial microstructure, the heat-affected zone, and the weld fusion zone. Since this study, we also observed that minimum weld diameter generally increases as the strength level of the steel increases, or strength ratio between weld and base material decreases (Ref. 4).

a weld button could always be produced during chisel test when appropriate process parameters were selected.

2. Weld times for incipient melting, beginning of expulsion, and complete elimination of interfacial fracture were correlated successfully to weld current and sheet thickness. This demonstrated that chemical composition and coating affected weld thermal history only within the scatter of the experimental data. The fact that interfacial fracture fully disappeared after a minimum weld time confirms that spot weld fracture was related primarily to weld thermal history.

3. Statistical formulas were developed to establish process maps for predicting weld fracture mode in 0.9- to 2.2-mm-thick DP600 steels. Process maps revealed that weld buttons could be reproduced over a wide range of process parameters for thin sheets (i.e., less than about 1.5 mm). This range of process parameters was found to decrease dramatically as sheet thickness increases.

4. Weld button diameter, ϕ , as a function of the weld current, I, weld time, t, and sheet thickness, d, was identified as the most important factor in spot weld fracture. Interfacial fracture was fully eliminated in DP600 steels when

$$\phi(\text{mm}) \geq 2.7d(\text{mm}) + 1.6$$

5. The minimum weld button diameters suggested from this study were often comparable to weld buttons suggested by Japanese (JIS Z3140) and German (DVS 2323) standards, particularly for the thicker gauges.

Conclusions

1. For all the DP600 steels of this study,

References

1. ULSAB-AVC Consortium, Technical

Transfer Dispatch #6 (Body Structure Materials), May 26, 2001.

2. Svensson and Larsson, J. K. 2002. *Steel World* 7: 21–26.

3. Marya, M., and Gayden, X. Q. 2005. Development of requirements for resistance spot welding dual-phase DP600 steels part 1 — The causes of facial fracture. *Welding Journal* 84(11): 172-s to 182-s.

4. Marya, M., Hector, L. G., Wang, K., and Gayden, X. Q. 2005. *ASME Journal of Manufacturing Science and Engineering* (in press).

5. Chao, Y. J. 2003. *ASME Journal of Engineering Materials and Technology* 125: 125–132.

6. Olson, D. L., Edwards, G. R., Liu, S., and Frost, R. 1993. *ASM Handbook*, Volume 6: Welding and joining handbook, Materials Park, Ohio: ASM International.

7. Grong, O. 1997. *Metallurgical Modeling of Welding* (Materials Modeling Series), 2nd Edition, The Institute of Materials.

8. Hyperstat Online, <http://davidmlane.com/hyperstat/A51911.html>.

9. Gould, J. E. 1987. An examination of nugget development during spot welding, using both experimental and analytical techniques. *Welding Journal* 67(1): 1-s to 10-s.

10. General Motors Engineering Standards, *Automotive Resistance Spot Weld*, GM4488M (Aug. 1995).

11. Girvin, B., Paterson, W., and Gould, J. 2005. Effect of manufacturing variables on the effectiveness of spike tempering during spot welding advanced high strength steel. Technical presentation at AWS Convention and Show, Dallas, Tex.

12. Lee, A., and Nagel, G. L. 1988. SAE Technical Paper 880277.

13. Harlin, N., Jones, T. B., and Parker, J. D. 2003. *Journal of Materials Processing Technology* 143/144: 448–453.

14. Japanese Industrial Standard, *Method of Inspection for Spot Welds*, JIS Z 3140 (1989).

15. German Standard, *Resistance Spot Welding*, DVS 2923.